Journal of Statistical Physics, Vol. 43, Nos. 3/4, 1986

Periodic and Aperiodic Regimes in Coupled Dissipative Chemical Oscillators

Igor Schreiber,[1] Martin Holodniok,[2] Milan Kubíček,[3] and Miloš Marek[1]

Received May 31, 1985; final January 2, 1986

Dynamic behavior of two identical reaction cells with linear symmetric coupling is studied in detail. The standard model reaction scheme "Brusselator" is used as the description of the kinetics. The uncoupled cells can exhibit either a stable stationary state or stable periodic oscillations. A number of stationary and periodic oscillatory patterns arise as a result of the coupling. A nonhomogeneous spatio-temporal organization includes homoclinic and heteroclinic oscillations as well as chaotic regimes. Numerical continuation algorithms are used to determine the dependence of stationary and periodic solutions on parameters. Stable stationary nonhomogeneous regimes exist typically at intermediate levels of coupling intensity. The nonhomogeneous periodic solutions arise either via Hopf bifurcatios from stationary solutions or via period-doubling bifurcations from the homogeneous periodic solutions. The results obtained may serve as a standard for the study of the behavior of other coupled systems in which either a stable stationary state or stable oscillations exist in the single cell.

KEY WORDS: Nonlinear dynamic systems; coupled cells; bifurcations; dependence of solution on a parameter; oscillations; chaos.

1. INTRODUCTION

Coupled reaction cells with mutual mass exchange are standard model systems for the study of reaction–diffusion processes in living cells, tissues, chemical reactors, and various compartmental representations of

[1] Department of Chemical Engineering, Prague Institute of Chemical Technology, Suchbátarova 5, 166 28 Prague, Czechoslovakia.

[2] Computing Centre, Prague Institute of Chemical Technology, Suchbátarova 5, 166 28 Prague, Czechoslovakia.

[3] Department of Mathematics, Prague Institute of Chemical Technology, Suchbátarova 5, 166 28 Prague, Czechoslovakia.

0022-4715/86/0500-0489$05.00/0

physiological systems.[1–4] The system of coupled reaction cells with mutual mass exchange through common walls was also used for experimental explorations of various steady-state and time-dependent regimes. Thus, coexisting steady states in two cells[5a] and combinations of non-homogeneous steady states (Turing structures) in the system of up to seven cells[5b] as well as periodic and aperiodic time-dependent regimes in two-coupled cells[6] were reported.

The models of two coupled reaction-diffusion cells were until now mostly studied by direct numerical simulation of dynamic mass balances.[1–4,7,8] Recently, a systematic methodology for study of global properties of steady-state and transient solutions in similar systems was developed.[9] In this paper we discuss the results of detailed studies of various regimes observed in two identical reaction cells with the "Brusselator" kinetic scheme coupled by diffusion. We believe that the results of such a study can be of general validity for coupled dissipative oscillators.

2. MODEL

The model of two well-mixed reaction cells with linear diffusion coupling and the Brusselator reaction kinetic scheme is used as a standard model system for the discussion of dissipative structures in nonlinear chemical systems,[10] in the same way as the Lorenz model serves for the studies of chaotic behavior in simple models of turbulence.[11,12]

The model (cf. Fig. 1) can be written in the form

$$dX/dt = v(X) \tag{1a}$$

$$X = \begin{bmatrix} x_1 \\ y_1 \\ x_2 \\ y_2 \end{bmatrix}, \qquad v(X) = \begin{bmatrix} A-(B+1)x_1+x_1^2 y_1+D_1(x_2-x_1) \\ Bx_1-x_1^2 y_1+D_2(y_2-y_1) \\ A-(B+1)x_2+x_2^2 y_2+D_1(x_1-x_2) \\ Bx_2-x_2^2 y_2+D_2(y_1-y_2) \end{bmatrix} \tag{1b}$$

Here A, B are constant parameters and x_i, y_i $(i=1, 2)$ are dimensionless concentrations of reaction intermediates X and Y in the first and second cells. The parameters D_1 and D_2 define the intensity of mass exchange between the cells. In the numerical computations we set $A=2$, $D_1/D_2=q=0.1$ and study solutions of the system (1) in dependence on two parameters $B>0$, $D_1 \geqslant 0$. In the following, the system (1a, b) with $D_1=D_2=0$ and $x_1=x_2$, $y_1=y_2$ will be called the decoupled system.

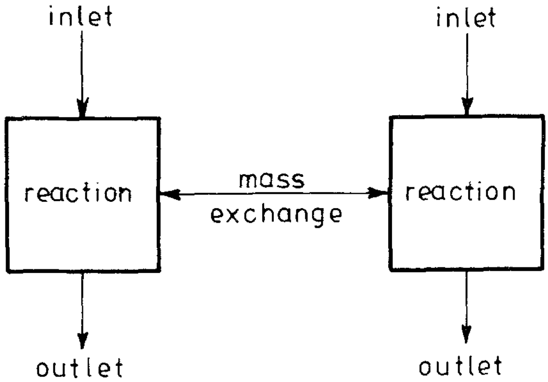

Fig. 1. Two reaction-diffusion cells with mutual mass exchange.

2.1. Symmetry in the Model

The choice of two identical cells (with respect to values of the parameters in the kinetic model) is reflected in the inherent symmetry of the vector field v.

It holds

$$v[\varphi(X)] = \varphi[v(X)], \qquad \varphi^2 = \mathrm{id} \tag{2}$$

where φ can be represented by a permutation matrix

$$\varphi = \begin{bmatrix} 0 & 0 & 1 & 0 \\ 0 & 0 & 0 & 1 \\ 1 & 0 & 0 & 0 \\ 0 & 1 & 0 & 0 \end{bmatrix} \tag{3}$$

exchanging the first component of the vector X with the third one and the second component with the fourth one. This corresponds to the exchange of cells. Hence, the orbits of (1) are mutually symmetric with respect to the symmetry plane Δ in the phase space $\mathbb{R}^4$, given by

$$\Delta = \{X \in \mathbb{R}^4;\, x_1 = x_2,\, y_1 = y_2\}$$

The orbits located in Δ will be called homogeneous, the others will be called nonhomogeneous.

The following qualitatively different types of orbits exist

1. Two distinct nonhomogeneous asymmetric orbits Γ and $\bar{\Gamma}$ exist such that $\bar{\Gamma} = \varphi(\Gamma)$ and $\Gamma = \varphi(\bar{\Gamma})$.

2. A single orbit Γ invariant with respect to φ exists and two possibilities arise, i.e., (a) a nonhomogeneous Δ-symmetric orbit exists, $\Gamma = \varphi(\Gamma)$, $\Gamma \notin \Delta$ (orbits of this type cannot be steady-state solutions) or (b) a homogeneous orbit exists, $\Gamma = \varphi(\Gamma)$, $\Gamma \in \Delta$ [orbits of this type are identical with those of decoupled system (1)].

2.2. Steady-State Analysis

Steady-state solutions satisfy

$$v(X) = 0 \tag{4}$$

It holds

$$x_1 + x_2 = 2A \tag{5a}$$

and for

$$u = x_1 - x_2$$

we obtain[13] either

$$u = 0 \tag{5b}$$

or u satisfies a biquadratic equation

$$q\omega u^4 + 4(B - 2A^2 q\omega + 2D_1\omega)u^2 + 16(A^4 q\omega - A^2 B + 2A^2 D_1 \omega) = 0 \tag{5c}$$

where $\omega = (D_1 + 0.5)/D_1$. Then

$$y_1 = \frac{2A(2B + q\omega u^2)}{4A^2 + u^2} - \frac{q\omega u}{2} \tag{5d}$$

$$y_2 = \frac{2A(2B + q\omega u^2)}{4A^2 + u^2} + \frac{q\omega u}{2} \tag{5e}$$

It follows from (5b) and (5c) that either one, three, or five steady-state solutions exist. The homogeneous solution S_H: $[x_1 = x_2 = A; y_1 = y_2 = B/A]$ lies in Δ and exists for all values of parameters. The nonhomogeneous solutions exist in asymmetric pairs S^1_N, $\bar{S}^1_\mathrm{N}$ and S^2_N, $\bar{S}^2_\mathrm{N}$ (Table I). All four nonhomogeneous solutions exist for parameter values satisfying[13]

$$\omega(4A\sqrt{D_1 q} - 2D_1) < B < \omega(A^2 q + 2D_1), \qquad 4D_1 < A^2 q \tag{6a}$$

Table I. Types of Steady-State and Periodic Solutions

Symbol	Type of solution	Homogeneity	Δ symmetry	Solution symmetric to the original one	Mutual phase relations in two cells	Remarks
S_{H}	Steady-state	Homogeneous	$S_{\mathrm{H}} \in \Delta$	$S_{\mathrm{H}} = \varphi(S_{\mathrm{H}})$		
S_{N}^1 S_{N}^2	Steady-state	Nonhomogeneous	Asymmetric	$\bar{S}_{\mathrm{N}}^1 = \varphi(S_{\mathrm{N}}^1)$ $\bar{S}_{\mathrm{N}}^2 = \varphi(S_{\mathrm{N}}^2)$		
P_{H}	Periodic	Homogeneous	$P_{\mathrm{H}} \in \Delta$	$P_{\mathrm{H}} = \varphi(P_{\mathrm{H}})$	Synchronized	Fig. 7e
P_{NA}	Periodic	Nonhomogeneous	Δ symmetric	$P_{\mathrm{NA}} = \varphi(P_{\mathrm{NA}})$	Antiphase	Fig. 7b Fig. 7c
P_{NI}	Periodic	Nonhomogeneous	Asymmetric	$\bar{P}_{\mathrm{NI}} = \varphi(P_{\mathrm{NI}})$	In-phase	Fig. 7d
P_{NO}	Periodic	Nonhomogeneous	Asymmetric	$\bar{P}_{\mathrm{NO}} = \varphi(P_{\mathrm{NO}})$	Out of phase	Fig. 7a

Two nonhomogeneous solutions exist for

$$B > \omega(A^2 q + 2D_1) \tag{6b}$$

The dependence of these nonhomogeneous solutions on B and D_1 is shown in Fig. 2. The solutions are characterized by means of the coordinate x_1; all points on the surface π in the space (x_1, B, D_1) represent the nonhomogeneous steady-state solutions. The symmetry of solutions with respect to Δ corresponds to the symmetry of π with respect to the plane $x_1 = A$. A cross section of surface π with plane $B = 5.9$ is shown in Fig. 3.

We obtain so called solution diagram, a dependence of the chosen norm of the solutions on one parameter, here D_1. Such a diagram can be generated by means of standard continuation algorithms.[9] It can be seen from Fig. 3 that nonhomogeneous steady-state solutions bifurcate from S_H via symmetry-breaking bifurcations, i.e., in pairs mutually symmetric with respect to Δ. The stability of steady-state solutions is also depicted in Fig. 3 (eigenvalues of the linearized system were evaluated to determine the stability).

The stability of S_{H} can be easily determined analytically. On linearizing (1) around S_{H} and solving the eigenvalue problem, the characteristic equation is

$$[\lambda^2 - (B - 1 - A^2)\lambda + A^2]\{\lambda^2 - [B - 1 - A^2 - 2D_1(1 + q^{-1})]\lambda + (1 + 2D_1)(A^2 + 2D_1 q^{-1}) - 2BD_1 q^{-1}\} = 0 \tag{7}$$

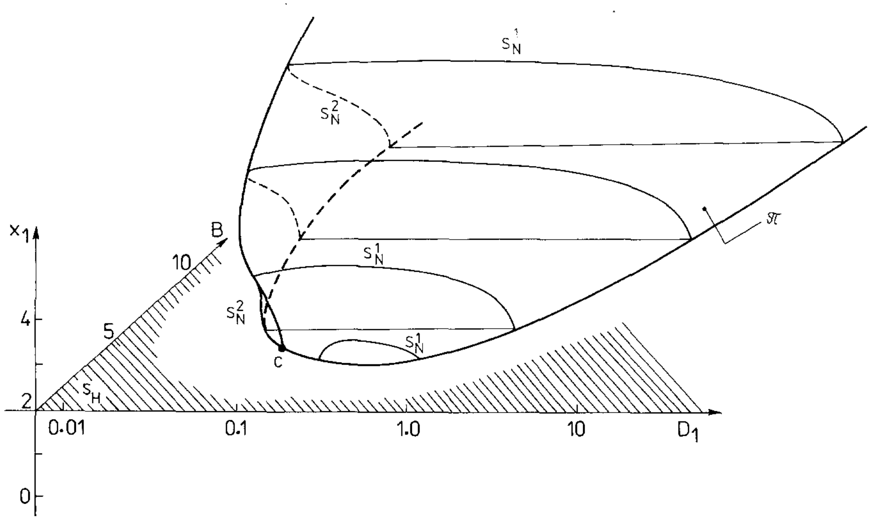

Fig. 2. Steady-state solutions in (x_1, B, D_1) space; the nonhomogeneous solutions lie on the surface π, which is symmetric with respect to the plane of homogeneous solutions $x_1 = A = 2$ (only the upper part of the solution surface is shown here). The solutions S_{N}^2 and $\bar{S}_{\mathrm{N}}^2$ arise at the cusp point C.

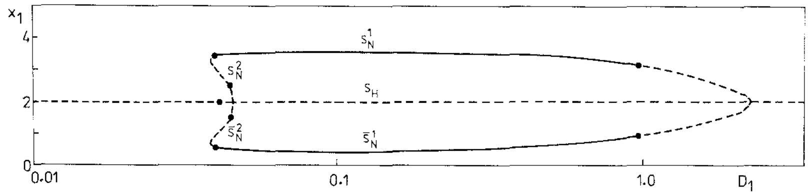

Fig. 3. Solution diagram of steady-state solutions (dependence of x_1 on D_1), $B = 5.9$. Full line—stable solution; dashed line—unstable solution; periodic solutions branch off at the Hopf bifurcation points denoted by ●, cf. Fig. 6.

Of special interest are bifurcations from S_H, occurring when an eigenvalue λ is either zero (appearance of nonhomogeneous steady-state solutions) or pure imaginary (appearance of a periodic solution called Hopf bifurcation). The loci of bifurcation points in the (B, D_1) parametric plane form curves which are together with the loci of points of bifurcation from non-

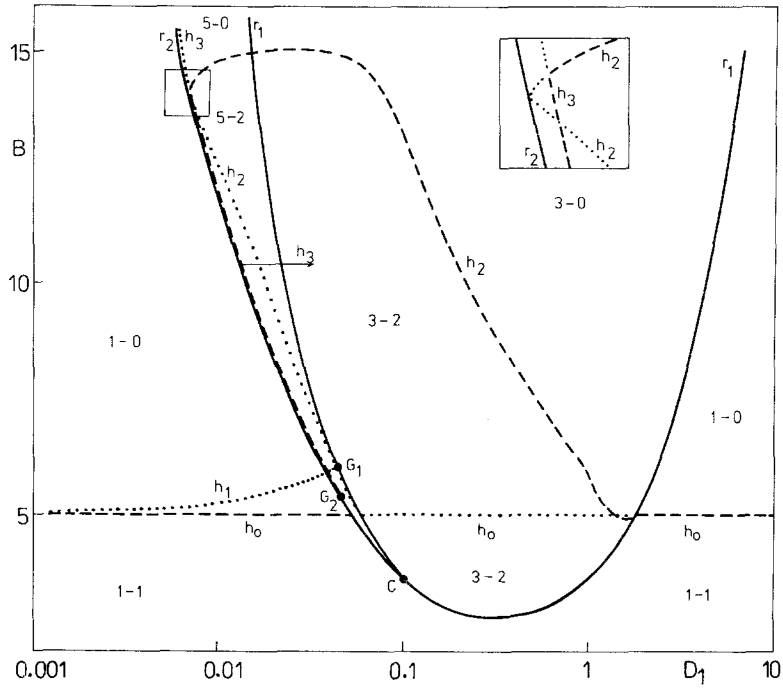

Fig. 4. Bifurcation diagram of steady-state solutions in the parametric plane (B, D_1). The plane is divided by the bifurcation curves into regions denoted by $m - n$, where m is the total number of solutions and n is the number of stable solutions. Full lines—limit points (curve r_2) or symmetry breaking bifurcations (curve r_1); dashed lines—Hopf bifurcations from stable steady-state solutions; dotted lines—Hopf bifurcations from unstable steady-state solutions. Curves of Hopf bifurcations, as well as degenerate bifurcation points G_1, G_2, are described in Section 3.2.

homogeneous steady-state solutions shown in Fig. 4. This so-called bifurcation diagram enables one to determine the number and stability of steady-state solutions in various regions of the parametric plane (B, D_1).

The condition for the symmetry breaking bifurcation from S_H is obtained from (7) when $\lambda = 0$, i.e.

$$B = \omega(A^2 q + 2D_1) \tag{8a}$$

(see curve r_1 in Fig. 4). The condition for the coalescence of S_N^1 with S_N^2 (and $\bar{S}_N^1$ with $\bar{S}_N^2$) at limit points can be obtained from (5c) by putting the discriminant equal to zero, i.e.

$$B = \omega(4A\sqrt{D_1 q} - 2D_1) \tag{8b}$$

(see curve r_2, Fig. 4). The description of Hopf bifurcation curves is given in Section 3.2.

It follows from the stability analysis that stable nonhomogeneous steady-state solutions may exist for a range of parameter values where the homogeneous solution S_H is not stable and/or when homogeneous oscillations may be expected. Similar behavior was observed in experiments with the Belousov–Zhabotinski reaction in two coupled cells.[14] An appearance of stable-steady states, when two oscillating cells are coupled, have been computed for several models by Bar–Eli.[15]

3. CLASSIFICATION OF PERIODIC SOLUTIONS AND THEIR BIFURCATIONS

According to the classification of orbits in Section 2.1, periodic solutions can be either nonhomogeneous (divided into asymmetric and Δ-symmetric solutions) or homogeneous. Note that the Δ-symmetric periodic oscillations with the period T imply the following phase relations

$$\begin{aligned} x_1[t + (T/2)] &= x_2(t) \\ y_1[t + (T/2)] &= y_2(t) \end{aligned} \tag{9}$$

i.e., both cells oscillate in opposite phases and hence the Δ-symmetric solution may be also called an "antiphase" solution.

It is useful to differentiate among the two types of asymmetric solutions according to the character of the mass exchange between the cells. The flux of the component X (or Y) can be either unidirectional or it can alternate, i.e., $\mathrm{sgn}(x_1 - x_2)$ or $\mathrm{sgn}(y_1 - y_2)$ is either constant or it alternates.

Based on the symmetry and on the character of the mass flux between the cells, the following classification of periodic solutions (P) can be made (cf. Table I)

(1) Homogeneous solution (P_H) with the orbit located in Δ (zero mass flux between the cells).

(2) Nonhomogeneous solutions:

(a) Δ-symmetric or antiphase solution (P_{NA}); the corresponding closed orbit is self-symmetric with respect to Δ and thus (9) holds. Here $\mathrm{sgn}(x_1 - x_2) = 1$ in one half of the period and $\mathrm{sgn}(x_1 - x_2) = -1$ in the other one; hence, the flux alternates.

(b) In-phase asymmetric solutions (P_{NI} if $x_1 > x_2$ and $\bar{P}_{NI}$ if $x_1 < x_2$); two closed orbits P_{NI} and $\bar{P}_{NI}$ are mutually symmetric with respect to Δ; the flux between cells is unidirectional.

(c) Out of-phase asymmetric solutions (P_{NO} if $x_1 > x_2$ in the larger part of the period and $\bar{P}_{NO}$ otherwise); opposite to the in-phase solutions, the flux between the cells alternates.

The periodic solutions (both stable and unstable) can be found numerically using an algorithm based on the transformation of the system (1) into a boundary value problem with mixed boundary conditions. This algorithm combined with an algorithm for the continuation of solutions in dependence on a parameter[9] was used for the computation of one parameter family of periodic solutions, cf. Appendix or Ref. (16).

The stability of the computed periodic solutions is determined on the basis of the eigenvalues μ (multipliers) of monodromy matrix M, which represents the linearized flow along the periodic orbit, using the characteristic equation

$$\det(M - \mu I) = 0$$

The characteristic multipliers are computed along the branch of periodic solutions; the computation is easily realized in combination with the above-mentioned continuation algorithm. One multiplier is always equal to $+1$ because the system (1) is autonomous. If all remaining multipliers are contained inside the unit circle, then the corresponding periodic solution is stable. If at least one multiplier lies outside the unit circle, the periodic solution is unstable.

3.1. Bifurcations of Periodic Solutions

The stability may change at the bifurcation points, where one of the multipliers computed along the branch of solutions crosses the unit circle.

We recognize the following types of bifurcation points (cf. Fig. 5):

(a) Type $(+1)$, $\mu = 1$: limit point on the dependence of periodic solutions on a parameter. The number of solutions changes by two when a parameter is varied. Both stable and unstable periodic solutions can coincide at this point (cf. Fig. 5a).

(b) Type (-1), $\mu = -1$: period doubling bifurcation point. A branch of solutions with double period branches off the original branch of

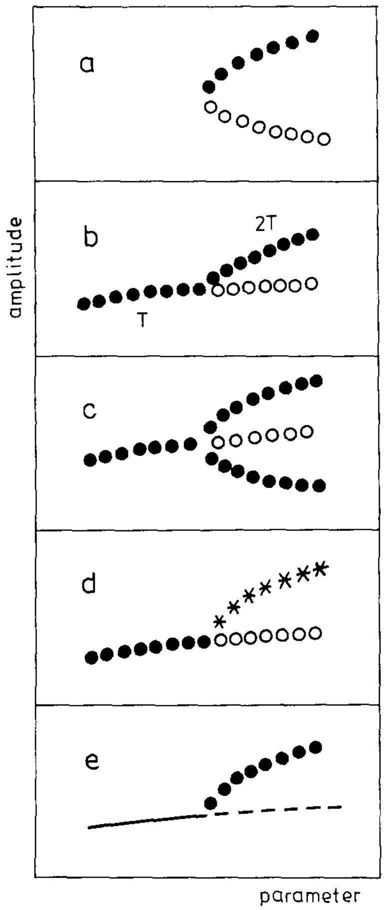

Fig. 5. Local bifurcation involving periodic solutions: (a) type $(+1)$—limit point; (b) type (-1)—period doubling; (c) type (SB)—symmetry breaking; (d) type (T)—torus bifurcation; (e) type (H)—Hopf bifurcation. Stable (unstable) steady-state solutions are denoted by full (dashed) lines, stable (unstable) periodic solutions by full (empty) circles, and tori by asterisks. Only bifurcations of stable solutions are shown, but bifurcations of unstable solutions from both stable and unstable branches may occur as well.

solutions. The continuation algorithm at such a bifurcation point continues along the original branch of solutions (cf. Fig. 5b). The new branch has $\mu = 1$ at the point of the bifurcation.

(c) Type (SB), $\mu = 1$: symmetry breaking bifurcation point. A pair of solutions mutually symmetric with respect to Δ bifurcates from a Δ-symmetric or a homogeneous periodic solution. This bifurcation can generically arise only in systems with inherent symmetry (cf. Fig. 5c).

(d) Type (T), $\mu_{1,2} = \omega_1 + i\omega_2$, $\omega_1^2 + \omega_2^2 = 1$, $\mu^n \neq 1$, $n = 1, 2, 3, 4$: bifurcation into an invariant torus (cf. Fig. 5d).

(e) Type (H): Hopf bifurcation, i.e., a bifurcation of the branch of periodic solutions from the branch of steady-state solutions (cf. Fig. 5e). It occurs at such points on the branch of steady-state solutions, where the matrix of linearization of the right-hand sides of (1), $\{\partial v/\partial x\}$, has a pair of purely imaginary eigenvalues.

The above types were numerically found in the system of two coupled cells studied in this paper. However, system (1) may also possess global bifurcations involving periodic solutions[17]; see Section 6.

According to Mallet-Paret and Yorke,[18] we define a branch of solutions as a continuous set of orbits in the space $\mathbb{R}^4 \times \mathbb{R}^1$ (i.e., in the product of the phase and parametric spaces—B, $D_1 \in \mathbb{R}^1$ are considered parameters) representing unique smooth dependence of both periodic solution and of the period on the parameter. Every two branches that have a common limit point belong to a family of solutions. Thus the family is a union of all such branches. The family of solutions may start (or terminate) at a Hopf bifurcation point, a period doubling bifurcation point, a symmetry breaking bifurcation point, or at a point where the period and/or amplitude tend to infinity. The family can be also formed by a closed cycle of branches (the first and the last branch are joined at the limit point). A single branch may also form a family. For example, applying the analogous definition to steady-state solutions, we have five branches S_H, S_N^1, S_N^2, $\bar{S}_N^1$, $\bar{S}_N^2$ and three families S_H, $S_N^1 \cup S_N^2$, $\bar{S}_N^1 \cup \bar{S}_N^2$ (cf. Figs. 2 and 3). This definition of the family can be extended to a higher-dimensional parameter space.

Every family of periodic orbits thus belongs to one of the six types—P_H, P_{NA}, P_{NI}, $\bar{P}_{NI}$, P_{NO}, $\bar{P}_{NO}$.

3.2. Hopf Bifurcation

The loci of all Hopf bifurcation points form smooth curves located on the surface of stationary solutions in (X, B, D_1) space. Projections of these curves into the plane (B, D_1) are shown in Fig. 4.

The Hopf bifurcation points for the family of homogeneous steady-state solutions S_H of (1) are determined using (7) by the relations

$$B = 1 + A^2 \tag{10a}$$

or

$$B = 1 + A^2 + 2D_1(1 + q^{-1}), \qquad B < \omega(2D_1 + qA^2) \tag{10b}$$

The relations (10a) and (10b) define for fixed A and q curves in the (B, D_1) parametric plane along which the Hopf bifurcations occur, cf. curves h_0 and h_1 in the Fig. 4, respectively.

The condition (10a) (curve h_0) corresponds to the bifurcation of P_H. We can easily check numerically that P_H exists always when $B > 1 + A^2$ (i.e., independently of the value of D_1) which is the consequence of the existence of periodic oscillations in a single isolated cell.

It follows from theoretical considerations on two symmetrically coupled oscillators[19] that condition (10b) (curve h_1) corresponds to the bifurcation of an unstable antiphase periodic solution P_{NA}. The continuation algorithm can be used starting close to the point of Hopf bifurcation; the method of asymptotic expansions may be used in the neighborhood of the Hopf bifurcation point[20] to obtain starting values of periodic solutions for the continuation algorithm.

If we admit equality in (10b) (cf. point G_1 in Fig. 4) then S_H is degenerate with double zero eigenvalue, which leads to a global Hopf bifurcation.[17]

Hopf bifurcation curves exist also on the families of nonhomogeneous solutions S_N. The curves h_2 and h_3 in Fig. 4 are composed from two parts, corresponding to a Hopf bifurcation from either a stable or unstable solution. Both parts of the curve h_2 start from points of a degenerate bifurcation with two purely imaginary and one zero eigenvalues. The unstable part goes through the S_N^2 branch, then reaches the S_N^1 branch via the limit point, and meets the stable part at the point with two pairs of purely imaginary eigenvalues. This point is the point of intersection of h_2 and h_3 and divides h_3 into stable and unstable parts as well. The curve h_3 extends on the S_N^1 branch very close to the curve r_2 of limit points and reaches this curve at the point G_2 with double zero eigenvalue.

Both h_2 and h_3 correspond to the bifurcation of in-phase periodic solutions. In addition, there exists a mirror image to each point on h_2 and h_3 with respect to Δ for a given B, D_1. Although the projection in Fig. 4 cannot distinguish between a solution and its mirror image, this can be done with the help of Fig. 2.

The curves h_2, h_3 were computed numerically in the following way.

First, a direct iteration technique[21] was used to locate a point of the Hopf bifurcation and then, starting from this point, the continuation algorithm[9] was utilized for the construction of the entire curve.

4. DEPENDENCE OF PERIODIC SOLUTIONS ON D_1

Let us take $A=2$, $q=0.1$, and $B=5.9$ and follow the dependence of periodic solutions on D_1. Under these conditions the corresponding single-cell system has an unstable stationary solution (corresponding to S_H) and a stable periodic solution (corresponding to P_H).

4.1. Periodic Solutions Originating at Hopf Bifurcation Points

From Fig. 3 we can infer that one point of the Hopf bifurcation from S_H and three symmetric pairs of the Hopf bifurcation points from S_N exist. The branches of periodic solutions are depicted in dependence on D_1 in the solution diagram in Fig. 6. The amplitude δx_1 of the concentration x_1 is taken as the norm, (T denotes period)

$$\delta x_1 = \max_{t \in [0,T]} x_1(t) - \min_{t \in [0,T]} x_1(t) \tag{11}$$

The following solutions arise at the points of Hopf bifurcation

(a) $D_1 \simeq 0.0409$: Unstable periodic solution P^1_{NA} branches off the solution S_H and continues in the direction of the increasing D_1.

(b) $D_1 \simeq 0.0382$: From the solution S^1_N (or from the symmetric solution $\bar{S}^1_N$) bifurcates unstable periodic solution P^3_{NI} (or $\bar{P}^3_{NI}$, respectively) to the right (cf. Fig. 11). These solutions are of the in-phase type.

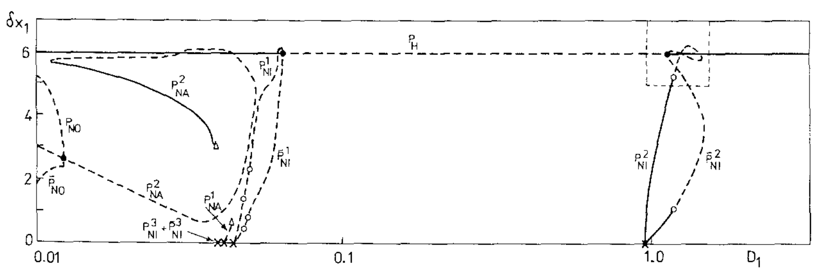

Fig. 6. Dependence of the amplitude δx_1 of several periodic solutions on D_1, $B=5.9$. Full lines—stable solutions, dashed lines—unstable solution, ×—Hopf bifurcations, ●—symmetry breaking bifurcations, ○—period doubling bifurcations, △—heteroclinic loops. No bifurcations occur at the other intersections of the lines. The complicated structure of solutions in the rectangle is shown in Fig. 8.

(c) $D_1 \simeq 0.0446$: Unstable solution P^1_{NI} ($\bar{P}^1_{\mathrm{NI}}$, respectively) branches off the solution S^2_{N} ($\bar{S}^2_{\mathrm{N}}$, respectively) to the right.

(d) $D_1 \simeq 0.9543$: Stable solution P^2_{NI} ($\bar{P}^2_{\mathrm{NI}}$, respectively) branches off the solution S^1_{N} ($\bar{S}^1_{\mathrm{N}}$, respectively) to the right.

The homogeneous periodic solution P_{H} has arisen by a Hopf bifurcation at $B = 5$, cf. (10b), and its amplitude is independent of D_1, cf. Fig. 6. The stability of P_{H} depends on D_1; there are two bifurcation points of the type (SB), where two mutually symmetric solutions P^1_{NI}, $\bar{P}^1_{\mathrm{NI}}$ and P^2_{NI}, $\bar{P}^2_{\mathrm{NI}}$ branch off the P_{H}. These families have arisen on the other side through Hopf bifurcations from S^2_{N}, $\bar{S}^2_{\mathrm{N}}$ and S^1_{N}, $\bar{S}^1_{\mathrm{N}}$. Hence they connect steady-state behavior with the periodic one. The symmetry breaking bifurcations cause the instability of P_{H} in the interval $0.063 \gtrsim D_1 \gtrsim 1.122$.

4.2. Weak and Intermediate Interaction

Examples of solutions for low and intermediate values of $D_1(D_1 \gtrsim 0.1)$ are depicted in Fig. 7. In addition to the branches arising through Hopf bifurcations (cases a–c in Sect. 4.1) we can observe also other periodic solutions denoted as P_{NO}, $\bar{P}_{\mathrm{NO}}$, P^2_{NA}. These solutions arise either through secondary bifurcations or through a primary bifurcation that is connected with the variation of other parameters than D_1.

The branch P^1_{NA} arising via Hopf bifurcation at $D_1 \simeq 0.0409$ apparently terminates at the point where the period tends to infinity. Numerical computations suggest that the branch P^1_{NA} disappears at a heteroclinic loop, cf. Section 5. Similar behavior occurs on the stable branch of the family P^2_{NA}, cf. Fig. 6. The origin of these two heteroclinic loops can be elucidated by varying parameter B, cf. Section 6. Two examples of periodic solutions from the family P^2_{NA} are shown in several projections in Fig. 7(b, c).

Antiphase solutions in this family, shown in Fig. 7b, have an interesting behavior at the limit $D_1 \to 0$. At $D_1 \simeq 0.012$ a pair of out-of-phase solutions P_{NO}, $\bar{P}_{\mathrm{NO}}$ bifurcates through a symmetry breaking bifurcation from P^2_{NA}. With decreasing D_1, the amplitudes of oscillations in both cells approach those in decoupled cells on this branch of the P^2_{NA} family but the phase shift is still equal to half of the period. The entire branch is unstable.

Solutions in the families P_{NO}, $\bar{P}_{\mathrm{NO}}$, cf. Fig. 7(a), approach for $D_1 \to 0$ such a state, where the oscillations in the first cell come close to single-cell oscillations, while the oscillations in the second cell are damped and approach the single-cell steady state. However, all these solutions are unstable.

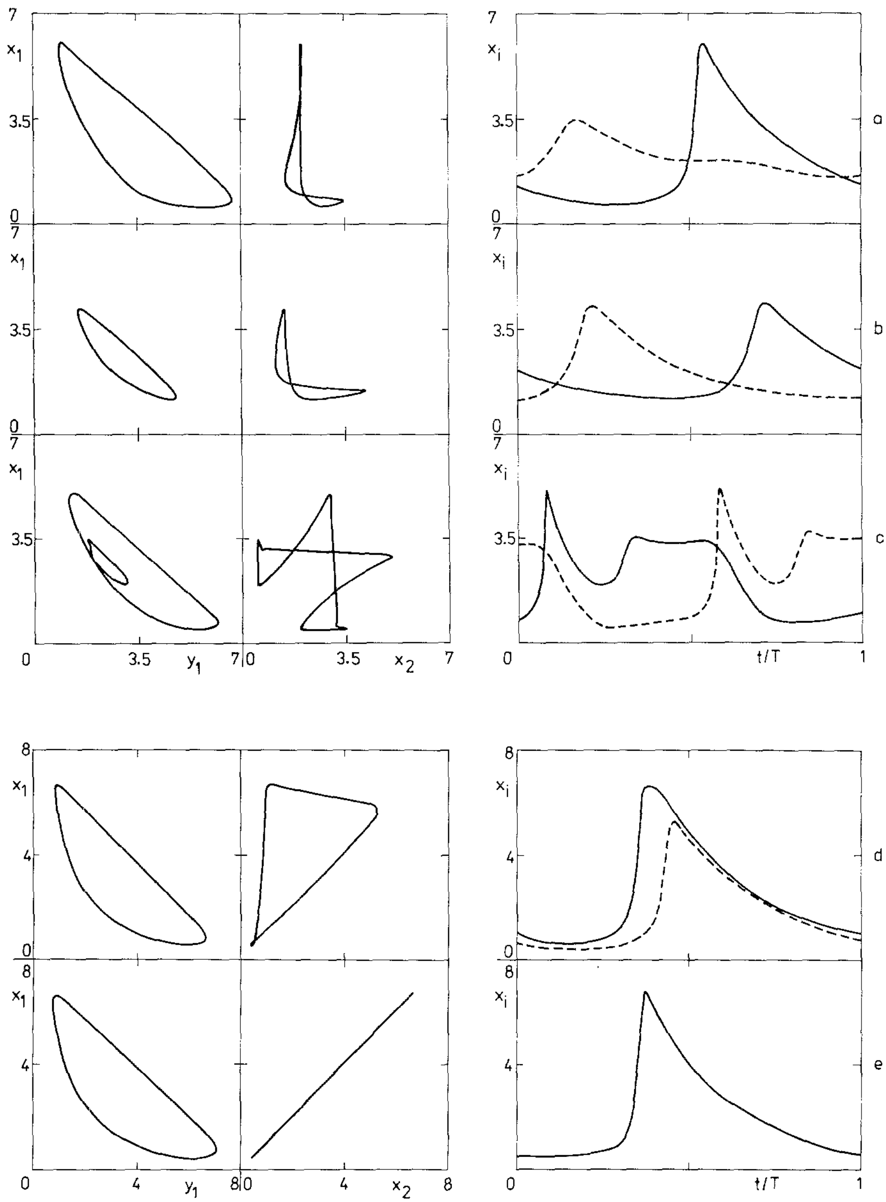

Fig. 7. Projections of the periodic orbits belonging to the region of weak and intermediate interaction into the planes (x_1, y_1), (x_1, x_2) and the time dependence of x_1 (full line) and x_2 (dashed line). $B=5.9$. (a) P_{NO}, $D_1=0.01$, $T=5.33102$; (b) P^2_{NA}, $D_1=0.01$, $T=4.45035$; (c) P^2_{NA}, $D_1=0.03$, $T=12.49991$; (d) P^1_{NI}, $D_1=0.0625$, $T=4.93383$; (e) P_H, D_1 arbitrary, $T=4.98652$.

Two stable periodic solutions P_H and P^2_{NA} coexist for $0.0112 \gtrsim D_1 \gtrsim 0.0383$ and stable steady-state solutions S^1_N, $\bar{S}^1_N$ coexist with the stable periodic solution P_H in the interval $0.03816 \gtrsim D_1 \gtrsim 0.063$. Hence in a small range of values of D_1 stable solutions P_H, P^2_{NA}, S^1_N, and $\bar{S}^1_N$ coexist.

The remaining solutions from the range of intermediate interactions are of the in-phase type and bifurcate via type (H) bifurcation. The asymmetric orbits P^1_{NI}, $\bar{P}^1_{NI}$, cf. Fig. 7(d), bifurcate to the right and finally annihilate at the point of type (SB) bifurcation. Both families are unstable and each contains two points of type (-1) bifurcation (newly bifurcating branches were not followed). The unstable families P^3_{NI}, $\bar{P}^3_{NI}$ branch off to the right and almost immediately terminate at two mutually symmetric homoclinic orbits; see Section 5.

4.3. Strong Interaction

A very complicated system of in-phase nonhomogeneous periodic solutions exists in the interval $0.9542 \gtrsim D_1 \gtrsim 1.4724$ (the interaction is an order of magnitude stronger now). The corresponding solution diagram (a part of the solution diagram from Fig. 6) is shown in Fig. 8. Let us denote

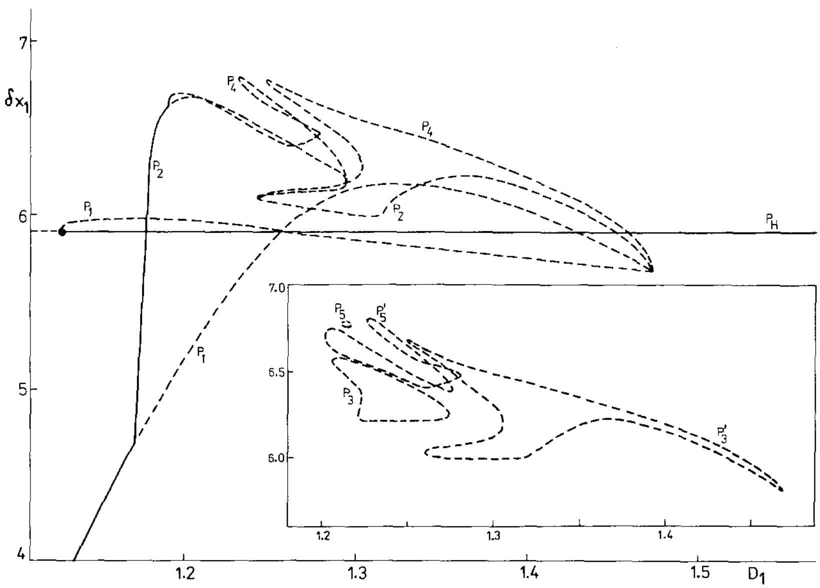

Fig. 8. Dependence of the amplitude δx_1 of periodic solutions $P_1, \ldots, P_5$ and P_H in the region of strong interaction. Full lines—stable solutions, dashed lines—unstable solutions; families of solutions are connected via period doubling bifurcations with the exception of type (SB) (denoted by ●) bifurcation connecting P_1 and P_H. Isolated families are shown separately.

each family in Fig. 8 by a symbol P_m, where m gives a number of local maxima on any coordinate of $X(t)$ within one period. In this notation the basic family P_{NI}^2 arising via type (H) bifurcation at $D_1 \simeq 0.9542$ is equivalent to P_1. Let us denote P_m^{s} that part of the family P_m, where the solutions are stable. To differentiate between the unstable parts of the family we make use of the empirical observation that for each unstable solution in the family P_m only one characteristic multiplier μ lies outside the unit circle. Let us denote $P_m^+ (P_m^-)$ that unstable part of P_m where $\mu > 0$ ($\mu < 0$). For simplicity we omit the symmetric images $\bar{P}_m$.

At point $D_1 \simeq 1.1720$ the family P_2 with a double period bifurcates from the basic family P_1; from the family P_2 bifurcates the family P_4 with a four-fold period (related to P_1), and so on. The intervals between the bifurcation values of D_1 for the subsequently bifurcating periodic solutions decrease geometrically with the universal quotient δ.[22] The sequence of the double period bifurcation points is oriented in the direction of the increasing D_1.

A similar sequence of the period doubling bifurcations begins also at the point $D_1 \simeq 1.4702$ close to the limit point on P_1; the subsequent bifurcation points are oriented in the direction of decreasing D_1. The family P_2 bifurcating at $D_1 \simeq 1.4702$ finally joins the family P_2 bifurcating at $D_1 \simeq 1.1720$. Two families P_4 bifurcate on this common P_2 family; both P_4 families return to the P_2 family. Altogether four families of P_8 solutions bifurcate from the two P_4 families, etc.

Several solution families (e.g., P_3 and P_5 in Fig. 8) form closed curves-isolas; cascades of the period doubling bifurcations may again start from the isolas. Any bifurcating family of solutions with the double period terminates again on the original isola (not shown in Fig. 8).

The stability changes and bifurcations on individual families of solutions occur usually in a very narrow range of the values of the parameter D_1 and thus they cannot be shown on the scale of the figure.

Each family P_m can be constructed by joining three types of branches, B_m^{s}, B_m^+, $B_m^{\mathrm{s-s}}$, which themselves are combinations of stable and unstable parts P_m^{s}, P_m^+, P_m^-, cf. Fig. 9. For example, the families P_2 and P_4 in Fig. 8 (i.e., the solutions which do not form isolas) arise via the combination $B_m^{\mathrm{s-s}} \cup B_m^+ \cup B_m^{\mathrm{s-s}}$; the isolas P_3, P_3', and P_5' can be formed via the combination $B_m^{\mathrm{s-s}} \cup B_m^+ \cup B_m^{\mathrm{s-s}} \cup B_m^+$ and P_5 via the combination $B_m^+ \cup B_m^{\mathrm{s}}$.

We may expect that the behavior of families P_m for higher values of m will be similar.

Periodic solutions for $D_1 = 1.26$ from the branches $B_1^{\mathrm{s-s}}$, $B_2^{\mathrm{s-s}}$, $B_3^{\mathrm{s-s}}$, $B_4^{\mathrm{s-s}}$, $B_5^{\mathrm{s-s}}$, and $B_6^{\mathrm{s-s}}$ are depicted in Figs. 10(a–f).

The structure of periodic solutions in the region of the strong interaction is very complex (it appears that an infinite number of solutions exist

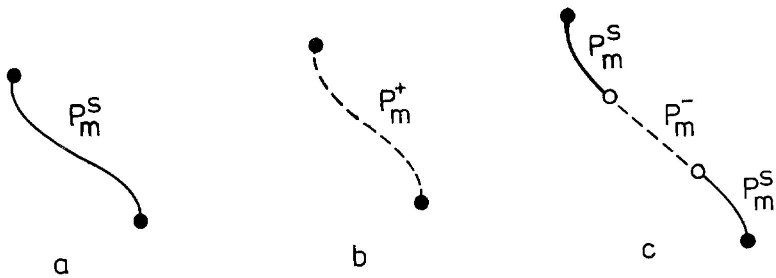

Fig. 9. Types of branches forming the families P_m. (a) stable branch B^s_m; (b) unstable branch B^+_m; (c) combined branch B^{s-s}_m with two period doubling bifurcation points. ○—period doubling bifurcation point; ●—points where the branches terminate (i.e., Hopf bifurcation points, limit points, symmetry breaking bifurcation points, period doubling bifurcation points).

here). On the contrary, the way in which new solutions originate and change their stability is simple, cf. Fig. 8. At the limit point a pair of solutions bifurcates through $(+1)$ bifurcation; one solution is stable and the second one is unstable. If a bifurcation of the type (-1) occurs on the stable branch, then a cascade of (-1) bifurcations is expected to follow and terminate at the accumulation point.[22] An interval on the D_1 axis where stable periodic solutions betwen the limit point and the corresponding accumulation point exist will be called window. The numerical computations suggest that in the range $1.193 \gtrsim D_1 \gtrsim 1.470$ infinitely many windows with infinitely many stable periodic solutions exist. At the same time it appears that at many values of D_1 no stable periodic solutions exist and complicated chaotic attractors are observed.[23] Chaos generated by a period doubling sequence repeatedly occurs between the neighboring windows. In addition, the windows sometimes overlap, which leads to a multiple attractor behavior.[23,24]

As the behavior of solutions of (1) in the chaotic region is well-approximated by a one-dimensional iterated map of an interval,[24] the existence of periodic solutions P_m with different m is given by Sharkovskii's sequence.[25]

5. PERIODIC SOLUTIONS WITH LARGE PERIOD

We have observed on several occasions that the period of oscillations computed along the followed branch evidently increase to infinity. This behavior is to be expected in the neighborhood of a homoclinic orbit or of a closed loop consisting of two (or more) interconnected heteroclinic trajectories. For example, the dependences of the period along the stable

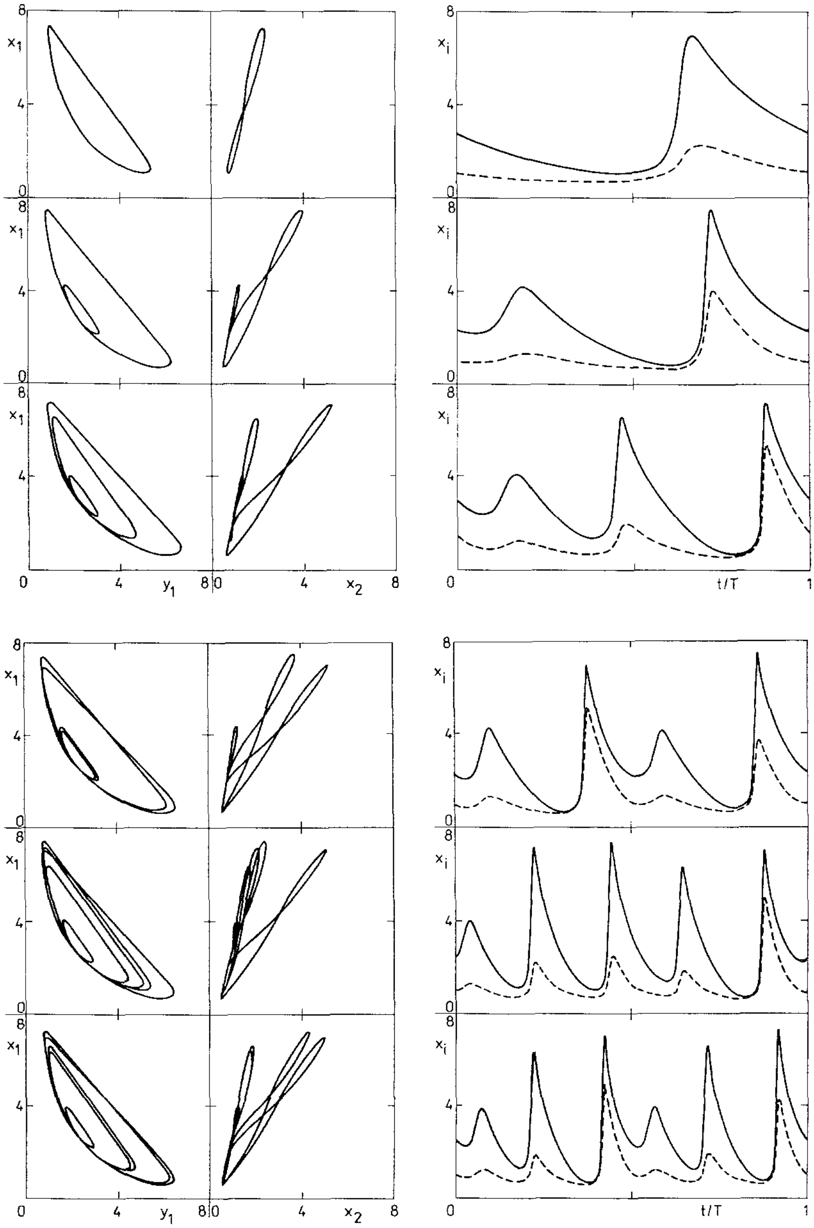

Fig. 10. Projections of the periodic orbits belonging to the region of strong interaction into the planes (x_1, y_1), (x_1, x_2) and the time dependences of x_1 (full line) and x_2 (dashed line); $B = 5.9$, $D_1 = 1.26$. (a) P_1, $T = 4.70783$; (b) P_2, $T = 8.40320$; (c) P_3, $T = 12.31918$; (d) P_4, $T = 16.61083$; (e) P_5, $T = 21.82897$; (f) P_6, $T = 24.93897$.

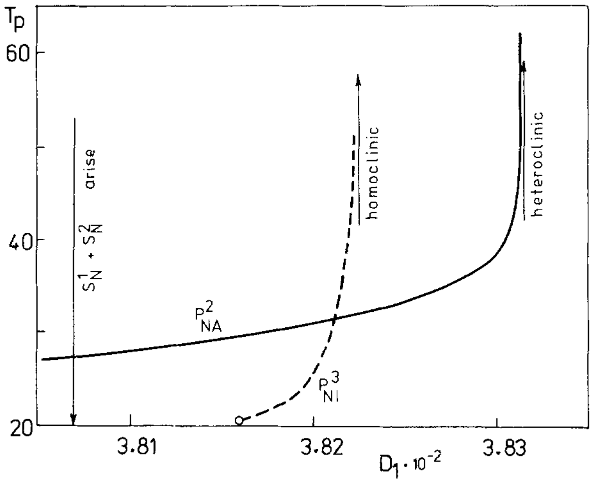

Fig. 11. Dependence of the period of solutions P^2_{NA} and P^3_{NI} on D_1, $B = 5.9$; stable branch P^2_{NA} approaches the heteroclinic loop, unstable branch P^3_{NI} approaches the homoclinic orbit.

branch of P^2_{NA} and along P^3_{NI} and $\bar{P}^3_{NI}$ on D_1 are shown for $B = 5.9$ in Fig. 11. The period increases fast with the increase of D_1.

A more detailed study of the development of periodic solutions on the branch P^2_{NA} reveals that the elongation of the period is caused by two gradually lengthening phases containing the phase points that are close to

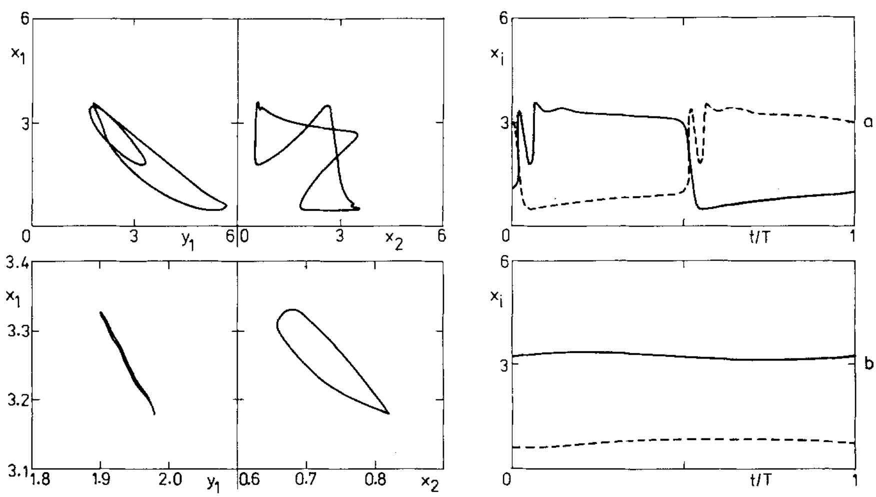

Fig. 12. Projections of the periodic orbits P^2_{NA}, P^3_{NI} close to the heteroclinic loop and the homoclinic orbit, respectively, into the planes (x_1, y_1), (x_1, x_2), and the time dependences of x_1 (full line) and x_2 (dashed line), $B = 5.9$. (a) P^2_{NA}, $D_1 = 0.03831651$, $T = 62.08770$; (b) P^3_{NI}, $D_1 = 0.03822041$, $T = 42.08532$.

the stationary states S_{N}^{2} and $\bar{S}_{\mathrm{N}}^{2}$, cf. Fig. 12(a). The phase point on the corresponding orbit stays at first for almost a half of the period close to $\bar{S}_{\mathrm{N}}^{2}$ and then rapidly jumps close to S_{N}^{2} and behaves in the same way due to the symmetry given by (2). Although it is not possible to continue P_{NA}^{2} further on from numerical reasons, we may assume that the solution P_{NA}^{2} approaches a heteroclinic loop between unstable steady states S_{N}^{2} and $\bar{S}_{\mathrm{N}}^{2}$. The same behavior occurs on the unstable branch of P_{NA}^{1}. A further description involves two parameter families of solutions and is given in the Section 6.

A limit case of the families P_{NI}^{3} and $\bar{P}_{\mathrm{NI}}^{3}$ are homoclinic orbits connected with steady states S_{N}^{2} and $\bar{S}_{\mathrm{N}}^{2}$. These periodic solutions branch off to the right through the Hopf bifurcation at $D_1 \simeq 0.038162$; cf. Fig. 11. At $D_1 = 0.038204$ the period of the solution is already very high and the solution cannot be continued by the algorithm.[16] The P_{NI}^{3} and $\bar{P}_{\mathrm{NI}}^{3}$ orbits have a very small amplitude and they are nearly planar; cf. Fig. 12(b).

Construction of homoclinic and heteroclinic orbits is currently the subject of intensive research, particularly for low-dimensional systems.[12,26] A general algorithm is also being developed in our research group.[27]

6. BEHAVIOR OF PERIODIC SOLUTIONS IN PARAMETRIC PLANE (B, D_1)

A numerical computation of two parameter families of periodic solutions was done sequentially by choosing several fixed values of the first parameter and continuing along the second parameter families. Thus the global picture is obviously incomplete and therefore it is presented only in a qualitative way, cf. Fig. 13(a–d). Nevertheless, with the exception of the possibly complicated behavior arising near several codimension two bifurcation points, we have obtained a rather clear picture of the behavior of solutions.

6.1. Groups of Families of Solutions

Families of periodic solutions can be divided into several groups which do not appear to intersect each other, i.e., the families within one group are not joined with the families of another group via loci of bifurcations. For example, one-parameter families for $B = 5.9$ (cf. Sects. 4 and 5) can be divided into five groups, cf. Fig. 6: (1) P_{NA}^{2}, P_{NO}, $\bar{P}_{\mathrm{NO}}$; (2) P_{NI}^{3}; (3) $\bar{P}_{\mathrm{NI}}^{3}$; (4) P_{NA}^{1}; (5) P_{H}, P_{NI}^{1}, $\bar{P}_{\mathrm{NI}}^{1}$, P_{NI}^{2}, $\bar{P}_{\mathrm{NI}}^{2}$, and all other solutions from the range of strong interaction. However, when the solutions are seen as dependent on B and D_1 the first, fourth and the fifth groups merge together, as will be explained later.

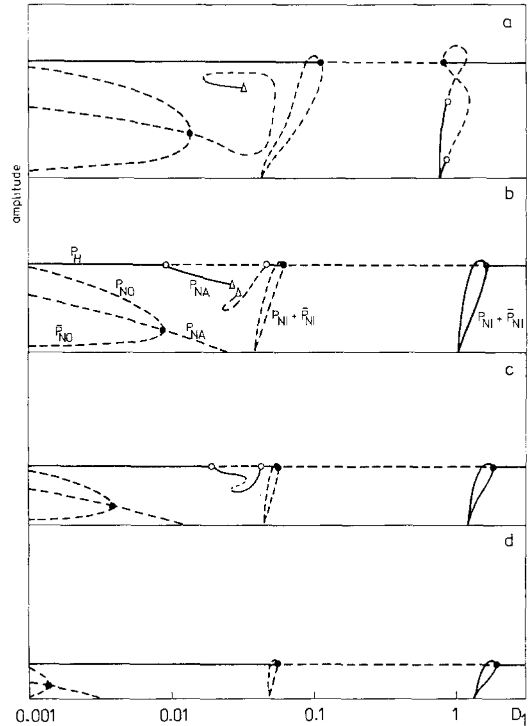

Fig. 13. Qualitative behavior of periodic solutions in the parametric plane (B, D_1) depicted as a sequence of the dependences of an amplitude on D_1 for different values of B; ○—period doubling bifurcations, ●—symmetry breaking bifurcations, △—heteroclinic loops. (a) $B \simeq 6.3$; (b) $B \simeq 5.5$; (c) $B \simeq 5.3$; (d) $B \simeq 5.1$.

Essentially all families within one group are mutually connected through bifurcations (except for some probably truly isolated families occurring, e.g., in the region of strong interaction). Thus starting from a chosen solution for given B and D_1 we can reach any solution in the same group by choosing a continuous path through the group. Let a primary family be that which starts from a steady-state solution via Hopf bifurcation and a secondary family be that which bifurcates from a primary family, etc.

6.2. Classification of Families of Solutions

Behavior of two-parameter families P^3_{NI} and $\bar{P}^3_{\mathrm{NI}}$ is relatively simple. For given B and D_1 the solutions from P^3_{NI} and $\bar{P}^3_{\mathrm{NI}}$ are mutual images under φ [cf. Eq. (2)] and although both families form two distinct groups, they can be treated simultaneously. They originate at the curve of the Hopf bifurcation points (cf. curve h_3 in the Fig. 4) from the nonhomogeneous solutions S^1_N, $\bar{S}^1_N$, respectively [two curves of the Hopf bifurcation points in the space $\mathbb{R}^4 \times \mathbb{R}^2$ merge together in the projection into the (B, D_1) plane]. The curves terminate at the critical point $G_2 \equiv (B \simeq 5.38276;$ $D_1 \simeq 0.04543)$ where two pure imaginary eigenvalues vanish. It seems that the results of Bogdanov[17] are directly applicable and we may conclude that a one-parameter family of homoclinic orbits (and its mirror image) arise at G_2. Numerical computations show that this curve extends very near to the Hopf bifurcation curve h_3 forming a very narrow cusp-shaped region of the existence of P^3_{NI} and $\bar{P}^3_{NI}$. The width of this region at $B = 5.9$ can be seen in Fig. 11.

All remaining families of solutions are interconnected via loci of bifurcations and form the third group. This group includes a very complicated structure of solution families originating from a primary ones which themselves originate at three curves of the type (H) bifurcation points (cf. curves h_0, h_1 and h_2 in Fig. 4).

The first Hopf bifurcation curve is given by (10a) and is associated with the appearance of the homogeneous solution P_H (cf. curve h_0 in Fig. 4). The bifurcation diagram for P_H in Fig. 14 shows two regions R_1 and R_2 of instability of P_H bounded by bifurcation curves. The boundary of R_1 is formed by a closed curve of type (-1) bifurcation points. The symmetry of the system implies that an antiphase solution P_{NA} with a double period will bifurcate along this curve,[28] cf. Fig. 13(b, c).

The one-parameter family originating along the boundary of R_1 is shown in Fig. 15 as a family depending on B for $D_1 = 0.02$. Using Fig. 6 we can conclude that this family is of the type P^2_{NA}. However, a chosen solution from the family P^1_{NA} (cf. Fig. 6) continued in dependence on B for

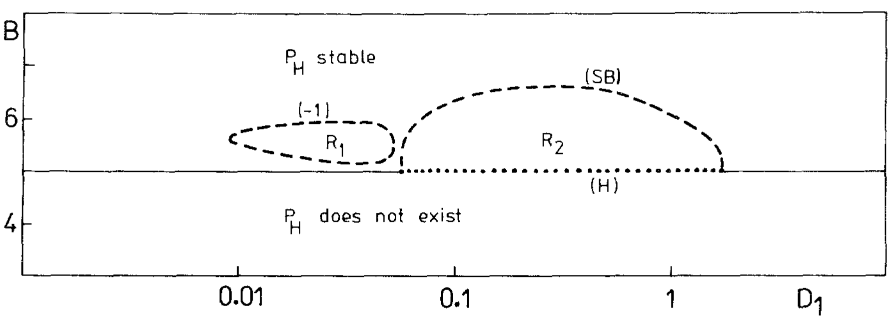

Fig. 14. Bifurcation diagram of the homogeneous periodic solution P_H in the (B, D_1) plane.

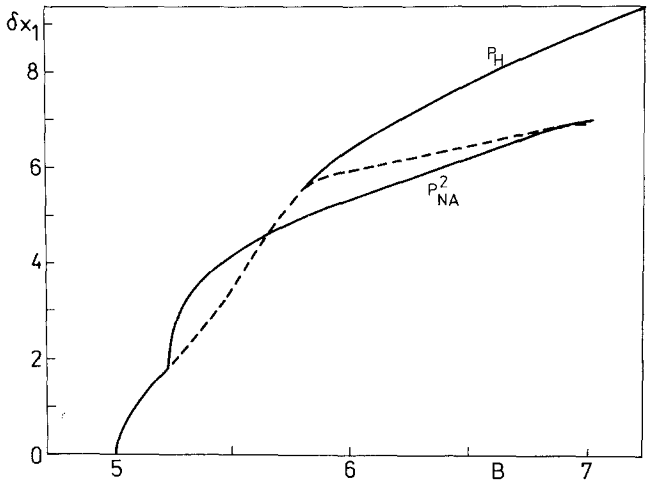

Fig. 15. Dependence of the amplitude δx_1 of the solutions P_H and P^2_{NA} on B, $D_1 = 0.02$.

fixed D_1 leads again to P^2_{NA}. It follows that P^1_{NA} and P^2_{NA} form a unique family (denoted by P_{NA}) when considered as dependent on B and D_1 simultaneously. This family bifurcates from P_H via period doubling bifurcation (cf. Fig. 14) and at the same time from S_H via Hopf bifurcation (cf. curve h_1 in Fig. 4). Hence P_{NA} is a primary family. The situation is schematically shown in Fig. 13(a-d), cf. also Fig. 6. Two heteroclinic loops described for $B = 5.9$ come close together if B is decreased and finally merge and disappear. The disappearance of one of both heteroclinic loops with increasing B is associated with the degenerate bifurcation point G_1, cf. Fig. 4. It is described in Section 6.3.

The boundary of R_2 is formed by two parts, the linear part of type (H) bifurcation points being at the same time a part of the line given by (10a) and the curve of the type (SB) bifurcation points. The symmetry of (1) implies that a pair of the in-phase solution families P_{NI}, $\bar{P}_{NI}$ will bifurcate along the (SB) curve, cf. Fig. 13(a–d).

Our numerical computations show that these families themselves bifurcate (or terminate) from two symmetric curves of the Hopf bifurcation points on a branch of nonhomogeneous steady states (cf. curve h_2 in Fig. 4). All solutions appearing via Hopf bifurcation from a nonhomogeneous steady state must necessarily be of the in-phase type, and this is in agreement with the branching of the in-phase solutions from the (SB) curve. Thus P_{NI} and $\bar{P}_{NI}$ are primary families, and they meet each other and at the same time intersect P_H at the (SB) curve of the boundary of R_2. The intersection is limited to $5 \gtrsim B \gtrsim 6.7$, cf. Fig. 14. Comparing these results with the solutions studied in Section 4 for $B = 5.9$, we are led to the conclusion that $P^1_{NI}(\bar{P}^1_{NI})$ from the region of intermediate interactions and $P^2_{NI}(\bar{P}^2_{NI})$ from the region of strong interactions are joined for $B \gtrsim 6.7$ and form a unique family (denoted by $P_{NI}(\bar{P}_{NI})$) when considered as two-parametric systems.

6.3. Period Doubling and Tori Bifurcations

The continuation algorithm[16] based on a simple shooting procedure was used in cases where the modulus of the largest multiplier was not too high. For very high values of the multiplier (approximately higher than 10^8) we switched to the multiple shooting algorithm. It appears that only small regions of stable nonhomogeneous periodic solution exists for $B \gtrsim 8$ and thus we did not follow this region in more detail. Instead, we studied two regions of the (B, D_1) plane containing two types of chaos.[23,29]

Fig. 16a contains a bifurcation diagram of the solutions P_{NI} in the (B, D_1) plane (see also Fig. 6, 8, 13a–d). P_{NI} is bounded by the curves of type (SB), (H) and (+1) bifurcation points and a bifurcating family with double period is bounded by the type (−1) bifurcation curve. Isolated families as well as potentially chaotic behavior exist inside the region boun-

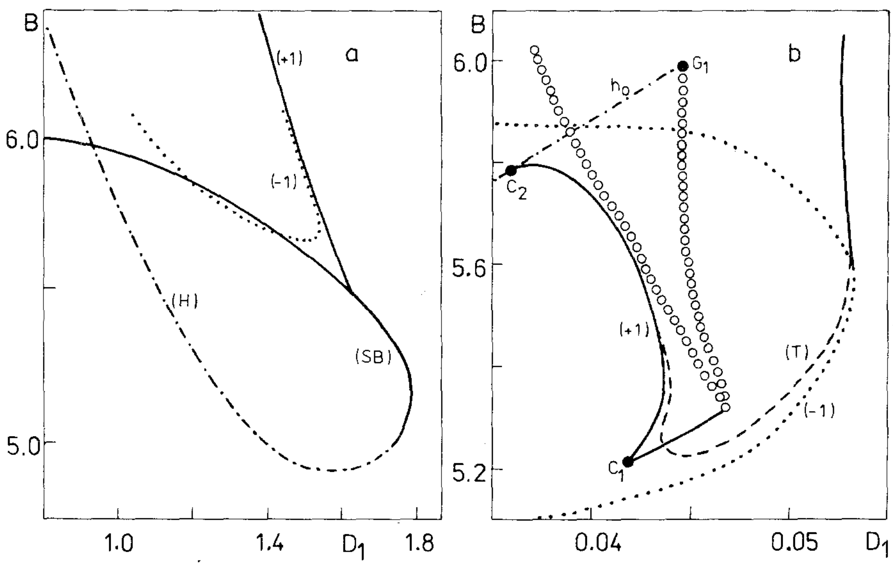

Fig. 16. Bifurcation diagram in the plane (B, D_1) for solutions P_{NI} (Fig. 16a) and P_{NA} (Fig. 16b). ···· – period doubling bifurcation curves; --- – torus bifurcation curve; –·–· – Hopf bifurcation curves; —— – limit point or symmetry breaking bifurcation curves; oooo – heteroclinic bifurcation curves.

ded by the curve of accumulation points of the period doubling sequences close to the type (-1) curve (not shown in the figure). Note that there is a region in the (B, D_1) plane such that stable nonhomogeneous oscillations exist for $B < 1 + A^2$, i.e., the interaction between the cells can lead to an oscillatory state even when the isolated cells possess no periodic solution (see also Ref. 30).

The second region of interest involves the bifurcation of tori from P_{NA}, cf. Fig. 16(b). The region of existence of P_{NA} is bounded by the curve of the type (-1) bifurcation points. In the cusp region bounded by two curves of the type $(+1)$ bifurcations there exist three different solutions (cf. Fig. 13c); two are stable and one is unstable close to the cusp point C_1. However, there exists another bifurcation changing the stability of P_{NA}—the bifurcation of type (T). P_{NA} is unstable inside the region formed by the (T) curve, and a large number of new periodic solutions associated with the phase-locked tori and with chaotic attractors arise.[29] According to general results,[31,33] the global picture of periodic solutions in this region is expected to be very complicated. A detailed numerical study might be of interest as very similar behavior including symmetries was recently observed in experiments.[32]

The curves of the limit points and of the tori bifurcations were computed using a modified algorithm.[9,16] To understand the global behavior of various branches of the P_{NA} family we also included curves along which the heteroclinic loops appear though they are computed with a limited accuracy. One of the curves of limit points emanating from C_1 splits into two curves of heteroclinic loops. One of these curves terminates at the point $G_1 \equiv (B \simeq 5.97979,\ D_1 \simeq 0.04454)$ where the stationary solution S_H has two zero eigenvalues. This point coincides with the end point of the Hopf bifurcation curve h_0 (cf. Fig. 4) and we may expect similar behavior as in the vicinity of the point G_2. However, due to the symmetry (2) the point G_1 does not fall into generic cases considered by Bogdanov.[17] This case was studied by Fiedler[17] who shows that a limiting case of periodic orbits with an infinite amplitude or period exists in the vicinity of G_1. The expected curve of homoclinic orbits is replaced by the curve of heteroclinic loops.

The second curve of limit points starting at C_1 terminates at the point C_2 which again lies on the curve h_0. The periodic solutions appearing along h_0 change the direction of the bifurcation at C_2.

7. CHAOTIC BEHAVIOR

Two different types of aperiodic (chaotic) solutions of (1) exist.[23,29] The first type exists in the region bounded by the curve of the (-1) bifurcation points in the bifurcation diagram in Fig. 16(a) and is closely connected with the complex structure of periodic solutions discussed in detail for the range $1.1933 \gtrsim D_1 \gtrsim 1.4724$, $B = 5.9$. A numerical simulation of (1) reveals that for the randomly chosen values of parameters from the above range the solution trajectory approaches either some periodic solution P_m (belonging to a window of periodic solutions) or a set of very complicated structure—a chaotic attractor.[23] All the solutions have always $x_1 > x_2$ (or $x_2 > x_1$); therefore, we may speak about an "in-phase chaos." This type of chaos appears through an infinite cascade of period doubling bifurcations.[22]

The second type of chaotic behavior arises through a sequence of bifurcations from a torus, which itself bifurcates from the antiphase periodic solution; hence, we may call it an "antiphase chaos." The structure of bifurcations leading to this type of chaotic attractor is complicated[29] and similar to the structure of bifurcations observed in some discrete maps in $\mathbb{R}^2$.[32,33]

If we choose a hyperplane Σ (three-dimensional) in the phase space, then the intersections of the chaotic trajectory with Σ will form a set, often called a Poincaré map, which characterizes a chaotic attractor. Typical Poincaré maps for both types of chaos are shown in Figs. 17(a, b).

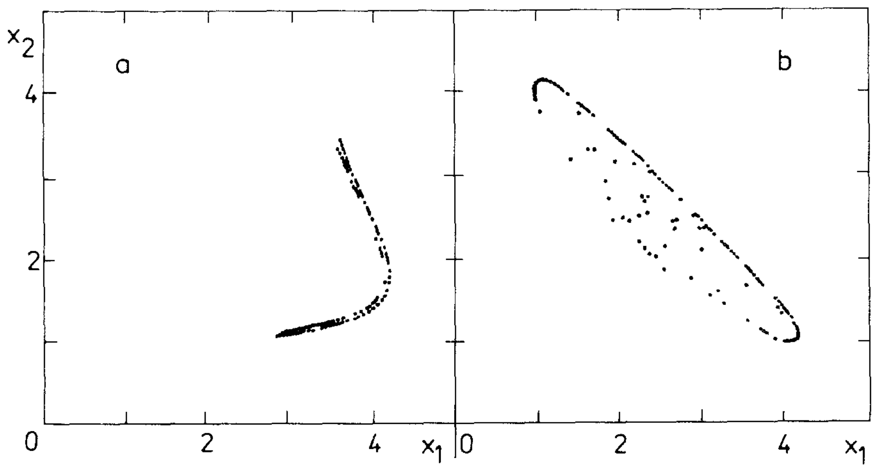

Fig. 17. Projection of the Poincaré maps of chaotic attractors into the plane (x_1, x_2). The surface of section Σ is defined as $\{(x_1, y_1, x_2, y_2);\ x_1 - y_1 + x_2 - y_2 = 2(A - B/A)\}$. (a) $B = 5.9$, $D_1 = 1.263$; (b) $B = 5.5$, $D_1 = 0.0521$.

8. DISCUSSION

In order to complete the picture of possible types of behavior of two coupled Brusselators, it is necessary to consider the variation of remaining parameters, $A > 0$ and $q \geqslant 0$. The changes of A do not lead to considerable changes of families of solutions, but the effect of variation of q is remarkable. The two-parameter families described in Section 6 ($A = 2$, $q = 0.1$) do not qualitatively change when q is decreased. All families exist even for $q = 0$ (the (B, D_1) plane must be now replaced by the (B, D_2) plane), including the in-phase and antiphase chaos and the heteroclinic and homoclinic behavior. On the other hand, the behavior is changed considerably when q is increased. This is caused by a successive shrinking and finally by a disappearance of both the Hopf bifurcation curve h_2 (cf. Fig. 4) and the bifurcation curves of types (-1) and (SB) (cf. Fig. 14). Thus all families of nonhomogeneous solutions from the fourth group disappear (including both types of chaos). Only the families P_{NA}, P_{NO}, $\bar{P}_{\mathrm{NO}}$, P^3_{NI}, $\bar{P}^3_{\mathrm{NI}}$, and P_{H} remain for $q \gtrsim 2$. However, it is not excluded that different families which do not occur for small q exist for higher values of q. This behavior was observed in a spatially continuous reaction–diffusion system.[36]

A different situation can be expected when two cells with different intrinsic frequencies are coupled together.[34] If the coupling is weak, the behavior is similar to that of the system (1) in the region of tori bifurcations. However, the nature of the appearance of torus is different.

9. CONCLUSIONS

The structure of solutions observed in a simple model of two linearly coupled cells with the Brusselator kinetic scheme is complicated. The model contains cubic nonlinearities and a simple symmetry and we may expect that a behavior of other types of linearly coupled oscillators described by models of the same structure may be also similar. Numerical methods used for construction of bifurcation and solution diagrams[9] may be efficiently applied in studies of global behavior of phase flows, as was illustrated on the studied example of coupled chemical oscillators. A similar approach, based on the continuation of solutions, we also successfully used in the analyses of the structure of both stable and unstable periodic solutions in the Lorenz model,[35] as well as in a compartmental model of a growth of a tissue.[37]

APPENDIX: COMPUTATION AND CONTINUATION OF PERIODIC SOLUTIONS

We present here a short description of an algorithm used for the computation and continuation of periodic solutions based on the shooting method, together with a continuation along the arclength of the solution locus. A detailed description of the algorithm is presented in Ref. 16.

We consider an autonomous system of ordinary differential equations (1)

$$\frac{dx}{dt} = v(x, \alpha) \tag{A1}$$

depending on a parameter α, $x = (x_1, x_2, ..., x_n)$. A periodic solution with the period T fulfils

$$x(T) = x(0) \tag{A2}$$

Considering the shooting method we choose initial conditions

$$x_i(0) = u_i, \qquad i = 1, 2, ..., n \tag{A3}$$

and the value of the period T. Then the system (A1) can be numerically integrated for fixed α from $t = 0$ to $t = T$. The values of the solution at $t = T$ are obtained from the integration as

$$x_i(T) = \psi_i(u_1, ..., u_n, T, \alpha), \qquad i = 1, 2, ..., n \tag{A4}$$

(they are dependent on the choice of $u_1, ..., u_n$, T, and α). The relation (A2) holds for any periodic solution; thus we have to satisfy n equations

$$F_i(u_1, ..., u_n, T, \alpha) = \psi_i(u_1, ..., u_n, T, \alpha) - u_i = 0 \qquad i = 1, 2, ..., n \tag{A5}$$

with $n + 1$ unknowns $u_1, u_2, ..., u_n$, T and one parameter α. We have to fix one variable except T. Let us fix u_k for some k. Our choice will be successful if on the trajectory of the kth component of the wanted periodic solution $x_k(t)$, $t \in [0, T]$, the chosen value u_k actually exists. Then we obtain a system (A5) of n nonlinear equations with n unknowns $U = (u_1, ..., u_{k-1}, u_{k+1}, ..., u_n, T)$ and one parameter α, which can be solved by the Newton method for fixed value of α. To obtain dependence of the solution $U(\alpha)$ on the parameter α we can use standard routine DERPAR[9] which is based on the continuation along the arclength of the solution and has predictor and corrector (Newton) parts. This continuation algorithm requires an evaluation of the functions F_i in (A5) and of the Jacobi matrix

$\partial F_i/\partial u_i$, $\partial F_i/\partial T$, $\partial F_i/\partial \alpha$. Elements of the Jacobi matrix can be determined on the basis of variational differential equations for variational variables

$$p_{ij}(t) = \partial x_i/\partial u_j, \qquad q_i(t) = \partial x_i/\partial \alpha \tag{A6}$$

These differential equations are obtained by differentiation of (A1) with respect to u_j and α. The elements of the Jacobi matrix of the system (A5) are defined as

$$\frac{\partial F_i}{\partial u_j} = p_{ij}(T) - \delta_{ij}, \qquad \frac{\partial F_i}{\partial T} = v_i[x(T), \alpha], \qquad \frac{\partial F_i}{\partial \alpha} = q_i(T) \tag{A7}$$

here δ_{ij} is the Kronecker delta. Thus we have all necessary information required by the continuation routine DERPAR and the continuation of the solution of the system (A5) for variables $u_1, \ldots, u_{k-1}, u_{k+1}, \ldots, u_n, T, \alpha$ can proceed until the fixed value of u_k "disappears" from the course of the periodic solution. To avoid this disappearance, the algorithm follows adaptively the deviation of the chosen u_k from the solution.

The stability of the computed periodic solution can be determined on the basis of characteristic multipliers, i.e., of eigenvalues μ of the monodromy matrix

$$M = \left\{ \frac{\partial \psi_i}{\partial u_j} \right\} = \{ p_{ij}(T) \} \tag{A8}$$

REFERENCES

1. J. I. Gmitro and L. E. Scriven, in *Intracellular Transport*, K. B. Warren, ed. (Academic Press, New York, 1966).
2. H. Martinez, *J. Theor. Biol.* **36**:479 (1972).
3. I. Prigogine and R. Lefever, *J. Chem. Phys.* **48**:1695 (1967).
4. R. A. Schmitz, in *Chemical Reaction Engineering Reviews*, M. H. Hulburt, ed. (American Chemical Society, Washington, D.C., 1975), p. 165.
5. I. Stuchl and M. Marek, *J. Chem. Phys.* **77**:1607 (1982a); **77**:2956 (1982b).
6. M. Marek and I. Stuchl, *Biophys. Chem.* **3**:24 (1975).
7. O. E. Rössler, *Z. Naturforsch.* **31a**:1168 (1976).
8. J. J. Tyson, *J. Chem. Phys.* **58**:3919 (1973).
9. M. Kubíček, *ACM Trans. Math. Software* **2**:98 (1976); M. Kubíček and M. Marek, *Computational Methods in Bifurcation Theory and Dissipative Structures* (Springer-Verlag, New York, 1983).
10. G. Nicolis and I. Prigogine, *Self-Organization in Nonequilibrium Systems* (John Wiley & Sons, New York, 1977).
11. E. N. Lorenz, *J. Atm. Sci.* **20**:130 (1963).
12. C. Sparrow, *The Lorenz Equations: Bifurcations, Chaos, and Strange Attractors* (Springer-Verlag, New York, 1982).

13. J. Tyson and S. Kauffman, *J. Math. Biol.* **1**:289 (1975); R. Lefever, *Bull. Cl. Sci. Acad. Roy. Belg.* **54**:712 (1968).
14. M. Marek, in *Synergetics—Far from Equilibrium*, A. Pacault and C. Vidal, eds. (Springer-Verlag, New York, 1979), p. 12.
15. K. Bar-Eli, *J. Phys. Chem.* **88**:3616 (1984); K. Bar-Eli, *Physica* **14D**:242 (1985).
16. M. Holodniok and M. Kubíček, *J. Comput. Phys.* **55**:254 (1984).
17. B. Fiedler, *Global Hopf Bifurcation of Two Parameter Flows*, preprint No. 293, University of Heidelberg, 1984; R. I. Bogdanov, *Trudy Sem. I. G. Petrovskogo* **2**:23 (1976a); **2**:37 (1976b), (in Russian); see also *Sel. Math. Sov.* **1**:373, 389 (1984).
18. J. Mallet-Paret and J. A. Yorke, *J. Diff. Eq.* **43**:419 (1982).
19. M. Kawato and R. Suzuki, *J. Theor. Biol.* **86**:547 (1980).
20. B. D. Hassard, *Numerical Evaluation of Hopf Bifurcation Formulae*, Report of the Department of Mathematics, State University of New York at Buffalo, 1978.
21. M. Kubíček, *SIAM J. Appl. Math.* **38**:103 (1980).
22. M. Feigenbaum, *J. Stat. Phys.* **19**:25 (1978); *J. Stat. Phys.* **21**:669 (1979).
23. I. Schreiber and M. Marek, *Physica* **5D**:258 (1982); I. Schreiber, M. Kubíček, and M. Marek, in *New Approaches to Nonlinear Problems in Dynamics*, P. J. Holmes, ed. (SIAM, Philadelphia, 1980), p. 496.
24. M. Marek and I. Schreiber, *Stochastic Behaviour of Deterministic Systems* (Academia, Praha, 1984), in Czech.
25. A. N. Sharkovskii, *Ukr. Mat. Z.* **16**:61 (Kiev, 1964); P. Štefan, *Commun. Math. Phys.* **54**:237 (1977).
26. V. N. Shtern and L. V. Shumova, *Phys. Lett.* **103A**:167 (1984); K. H. Alfsen and J. Frøyland, Systematics of the Lorenz Model at $\sigma = 10$, preprint (University of Oslo, Oslo, 1984).
27. M. Kubíček, A. Klíč, and M. Holodniok, in preparation.
28. A. Klíč, *Aplikace matematiky* **28**:5 (1983); J. W. Swift and K. Wiesenfeld, *Phys. Rev. Lett.* **52**:705 (1984).
29. I. Schreiber and M. Marek, *Phys. Lett.* **91A**:263 (1982).
30. J. C. Alexander, Spontaneous Oscillations in Two 2-Component Cells Coupled by Diffusion, preprint (University of Maryland, Maryland, 1984).
31. V. I. Arnold, *Geometrical Methods in the Theory of Ordinary Differential Equations* (Springer-Verlag, New York, 1983).
32. P. Bryant and C. Jeffries, *Phys. Rev. Lett.* **53**:250 (1984).
33. D. G. Aronson, M. A. Chory, G. R. Hall, and R. P. McGehee, *Commun. Math. Phys.* **83**:303 (1982).
34. M. Sano and Y. Sawada, *Phys. Lett.* **97A**:73 (1983).
35. M. Holodniok, M. Kubíček, and M. Marek, Stable and Unstable Periodic Solutions in the Lorenz Model (Technische Universität München, Technical report TUM-M 8217, Munich 1982).
36. P. Raschmann, M. Kubíček, and M. Marek, in *New Approaches to Nonlinear Problems in Dynamics*, P. J. Holmes, ed. (SIAM, Philadelphia, 1980), p. 271.
37. I. Schreiber, M. Kubíček, and M. Marek, *Z. Naturforsch.* **39c**:1170 (1984).